Interfacial Electric Field Modulation of 1D/2D $FeCo_2O_4$/g-C_3N_4 Heterostructures for Lithium Sulfur Batteries Over Wide Temperatures

Mengqing Wang,[a,b] Caixiang Wang,[a,b] Qin Tang,[b] Baojun Hou,[b] Zhenjie Cheng,[*a] Tengfei Duan,[*c] Lu Wang,[*d,e] Manfang Chen[*b]

[a] Zhejiang Key Laboratory for Island Green Energy and New Materials, School of Materials Science and Engineering, Taizhou University, Taizhou 318000, Zhejiang, P. R. China

[b] National Base for International Science & Technology Cooperation of New Energy Equipment, Energy Storage Materials and Devices; School of Chemistry, Xiangtan University, Xiangtan 411105, Hunan, P. R. China

[c] School of Materials Science and Engineering, Hunan Key Laboratory of Electrochemical Green Metallurgy Technology, Hunan University of Technology, Zhuzhou 412007, Hunan, P. R. China

[d] Key Laboratory of Green and Precise Synthetic Chemistry and Applications Ministry of Education, College of Energy Science and Engineering, Huaibei Normal University, Huaibei 235000, Anhui, P. R. China

[e] School of Materials Science and Engineering, Shandong University, Jinan 250061, Shandong, P. R. China.

[*] E-mail: (M. F. Chen) mfchen@xtu.edu.cn; (L. Wang) wanglu@chnu.edu.cn; (Z. J. Cheng) zjcheng@tzc.edu.cn

1. Experimental section

1.1 Chemicals and Materials

Cobalt nitrate hexahydrate ($Co(NO_3)_2·6H_2O$, AR grade, 99%), iron(III) nitrate nonahydrate ($Fe(NO_3)_3·9H_2O$, AR grade, 99%), urea ($CO(NH_2)_2$, 99%), ammonium fluoride (NH_4F, 98%), and melamine ($C_3H_6N_6$, 99%) were all purchased from Macklin Biochemical. All chemical reagents were used as received without further purification.

1.2 Synthesis of g-C_3N_4.

9 g of melamine were placed in a covered ceramic boat, heated in air from room temperature to 500 °C at a heating rate of 10 °C per minute, held for 2 h, and then cooled to room temperature to obtain a light-yellow solid.

1.3 Synthesis of $FeCo_2O_4$.

0.476 g of $Co(NO_3)_2·6H_2O$, 0.404 g of $Fe(NO_3)_3·9H_2O$, 0.901 g of $CO(NH_2)_2$, and 0.222 g of NH_4F were stirred and dissolved in 60 mL of deionized water. Then, the mixed solution was transferred into a 100 mL high-pressure autoclave and maintained at 120 °C for 12 h. After cooling, washing, and drying, the product was heated in a tube furnace at 400 °C for 2 h under an air atmosphere to obtain $FeCo_2O_4$ nanorods.

1.4 Synthesis of $FeCo_2O_4$/g-C_3N_4.

0.200 g of g-C_3N_4 and 0.010 g of $FeCo_2O_4$ were placed in 10 mL of ethanol and ultrasonically dispersed for 30 minutes. After drying, the resulting sample was heated at 550 °C for 1 h under a nitrogen atmosphere to prepare the $FeCo_2O_4$/g-C_3N_4 heterojunction.

1.5 Material characterization

An X-ray diffractometer (XRD, D8 Advances, Bruker, Germany) was used to determine the crystal structure of g-C_3N_4 and $FeCo_2O_4$/g-C_3N_4. To investigate the surface chemical component, X-ray photoelectron spectroscopy (XPS, ESCALAB Xi^+, Thermo Scientific, USA) was used. The structure and morphology of the as-prepared materials were investigated using scanning electron microscopy (SEM, JSM-6610LV, Japan; TESCAN MIRA3, Czech Republic) and transmission electron microscopy (TEM, JEM-2100F, Japan). In order to determine the specific surface area and pore size distribution, N_2 isothermal adsorption/desorption data were collected by a static physical adsorption apparatus (BK-112, China).

1.6 Synthesis of $FeCo_2O_4$/g-C_3N_4 separators

The polyvinylidene fluoride (PVDF) and conductive carbon dark (SP) were combined with the $FeCo_2O_4$/g-C_3N_4 at a weight ratio of 1:2:7. The $FeCo_2O_4$/g-C_3N_4 coated membranes were obtained by mixing well in N-methylpyrrolidone (NMP) solution and then coated on Celgard polypropylene (PP) film. g-C_3N_4 coated membranes were prepared using the same technique. The functional layer of the separator with a loading of approximately 0.58 mg/cm^2.

1.7 Preparation of Cathode

Carbon nanotubes (original from Cnano Technology) and sublimed sulfur were typically combined uniformly in a weight ratio of 7:3 and heated at 155 ℃ for 12 h to produce CNT/S. CNT/S, PVDF and conductive Super P mixed uniformly at a weight proportion of 7:2:1 in a NMP solution to obtain the slurry of cathode electrodes. The slurry was evenly coated on the charcoal coated aluminum foil. The foil was dried at

60 ℃ for 12 h in the vacuum and cut into disks with a diameter of 10 mm and a sulfur load of 1.40 mg/cm^2. Cathodes with higher sulfur loadings (4.41 mg/cm^2 and 6.42 mg/cm^2) were obtained by coating a slurry onto carbon paper (Toray origin).

1.8 Preparation of the Li_2S_8 Solution, Li_2S_6 Solution and Related Batteries.

S and Li_2S were mixed well in a molar ratio of 5:1 and then dissolved in the DOL/DME (v/v = 1/1) solution to obtain the 0.1 M solution of Li_2S_6, which was used as the electrolyte for the symmetric cell. The electrodes for the symmetric cells were prepared by homogenizing a mixture of catalytic materials (g-C_3N_4 and $FeCo_2O_4$/g-C_3N_4) without S and PVDF (mass ratio = 9:1). CV curves of symmetric cells were recorded at a scan rate of 10 mV/s and a voltage range of -1.0 to 1.0 V. The cell for testing the precipitation and dissolution of Li_2S was made in a similar way to a normal cell, but the electrolyte was the prepared Li_2S_8 solution. S and Li_2S were mixed well in a molar ratio of 7:1 and then dissolved in the DOL/DME (v/v = 1/1) solution to obtain the 0.1 M solution of Li_2S_8. The cell was discharged at a constant current of 0.112 mA to 2.06 V and then at a constant voltage of 2.05 V to observe the corresponding current−time curve. Li_2S dissolution experiments were performed by discharging the battery completed with Li_2S deposition experiments to 1.7 V at constant current at 0.112 mA and then charging it at a constant voltage of 2.4 V and observing the time−current curve.

1.9 Measurements of the galvanostatic intermittent titration technique (GITT).

A protocol involving a current pulse at 0.1 C for 10 minutes followed by 60 minutes of rest was utilized. The internal resistance could be quantified by the following relation equation:

$$\Delta R_{internal}(\Omega)=|\Delta iR|/I_{applied} \quad \text{S1}$$

Where ΔE is the voltage difference between the quasi-open-circuit voltage and closed-circuit voltage points, and $I_{applied}$ is the applied current.

1.10 Electrochemical Measurements

Cathodes with sulfur loadings of 1.40 mg/cm^2, 4.41 mg/cm^2, and 6.42 mg/cm^2 were prepared by mixing the synthesized material, conductive carbon Super P, and polyvinylidene fluoride (PVDF) in a mass ratio of 7:2:1. CR2025 coin cells were assembled using the cathode, a separator (Celgard 2400), an anode (lithium metal), and an electrolyte. The electrolyte consisted of a 1,3-dioxolane/1,2-dimethoxyethane (DOL/DME, v/v=1/1) solvent mixture, 1 M lithium bis (trifluoromethane) sulfonyl imide (LiTFSI), and 1 wt% lithium nitrate ($LiNO_3$). The electrolyte volume used was 30–40 μL. The E/S ratio for the high-sulfur-loading cells was 8 μL/mg and 6 μL/mg for sulfur cathodes of 4.4 mg cm^{-2} and 6.4 mg cm^{-2}, respectively. Galvanostatic charge-discharge tests were performed within a voltage range of 1.7–2.8 V using a battery testing system (Neware CT-4800T). Cyclic voltammetry measurements were conducted on a CHI 660E instrument at stated scan rates, generally for 0.1 0.2 0.3 0.4 0.5 mv/s. Electrochemical impedance spectroscopy (EIS) was recorded on a CHI 660E instrument over a frequency range of 10^5 Hz to 10^{-2} Hz.

The Randles-Sevcik equation:

$$I_p=2.69\times10^5 n^{3/2}AD_{Li^+}^{+1/2}C_{Li^+}v^{1/2} \quad \text{S2}$$

where the peak current is denoted by I_p, the number of electrons in the response is denoted by n, the cathode area (0.785 cm^2) is denoted by A, the Li^+ diffusion coefficient is denoted by D_{Li^+}, the electrolyte Li^+ concentration is denoted by C_{Li^+}, and the rate is denoted by v.

1.11 Preparation of the In Situ UV−vis Experiment.

The same methods as before are used to prepare materials for cathodes that contain S. The In Situ UV−vis cells were constructed in an Ar-filled glovebox utilizing a specially manufactured in situ cuvette (bought from Tianjin Aida Hengsheng Technology Development Co., LTD) with pristine g-C_3N_4/S and $FeCo_2O_4$/g-C_3N_4/S electrode as the cathode and Li metal as the anode. On an electrochemical workstation, the in situ cuvette cell was galvanostatically discharged at 0.05 C. From the start of the discharge until the end of the discharge, UV−vis spectra with a wavelength range of 400 − 750 nm were recorded for batteries, and the spectra were collected continuously. (High S areal loading: 4.39 mg/cm^2) The transformation process of S species is as follows:

$$S_8+2e^- \rightarrow S_8^{2-} \quad \text{S3}$$

$$S_8^{2-} \rightarrow S_6^{2-}+1/4S_8^{2-} \quad \text{S4}$$

$$S_6^{2-} \rightarrow 2S_3^{-} \quad \text{S5}$$

$$S_3^{\cdot-}+2e^- \rightarrow S_3^{2-} \quad \text{S6}$$

$$2S_3^{\cdot-}+2S_3^{\cdot-} \rightarrow 3S_4^{2-} \quad \text{S7}$$

$$S_8^{2-}+2e^- \rightarrow 3S_4^{2-} \quad \text{S8}$$

1.12 Density functional theory calculations

All spin-polarized calculations were performed using the Vienna *ab initio* simulation package (VASP)[1-2] based on density generalized function theory (DFT). The electron exchange correlation was described by the gradient-corrected Perdew-Burke-Ernzerh (GGA-PBE) functional.[3] Ion-electron interaction was described by the projector augmented-wave (PAW) method.[4] We built a heterojunction model consists 1×1×1 supercell $FeCo_2O_4$ (311) surfaces and 3×4×1 supercell g-C_3N_4, totaling 504 atoms. The cutoff energy was set to be 450 eV, and the total energy and force convergence for geometric optimization was set to 10^{-5} and 0.01 eV/Å, respectively. Integration in the Brilliouin zone was performed based on the Monkhorst-Pack scheme using a Γ centered 2×1×1 k-point mesh in each primitive lattice vector of the reciprocal space for optimization. The vacuum layer was set to 20 Å and a semi-empirical correction of DFT-D3[5] was adopted to account for the interaction of van der Waals forces. Charge density difference[6] analysis was performed to qualitatively describe the differences of charge distribution between polysulfides and substrates.

The adsorption energy ($\boldsymbol{E}_{ad}$) of Li_2S_6 on $FeCo_2O_4$ (311) and g-C_3N_4 surfaces can be written as

$$E_{ad} = E_{(sub + Li_2S_6)} - E_{(sub)} - E_{(Li_2S_6)}$$

$E_{(sub + Li_2S_6)}$ is the total energy of Li_2S_6 adsorbed on the substrate. $E_{(sub)}$ is the total energy of substrate $E_{(Li_2S_6)}$ is the total energy of Li_2S_6.

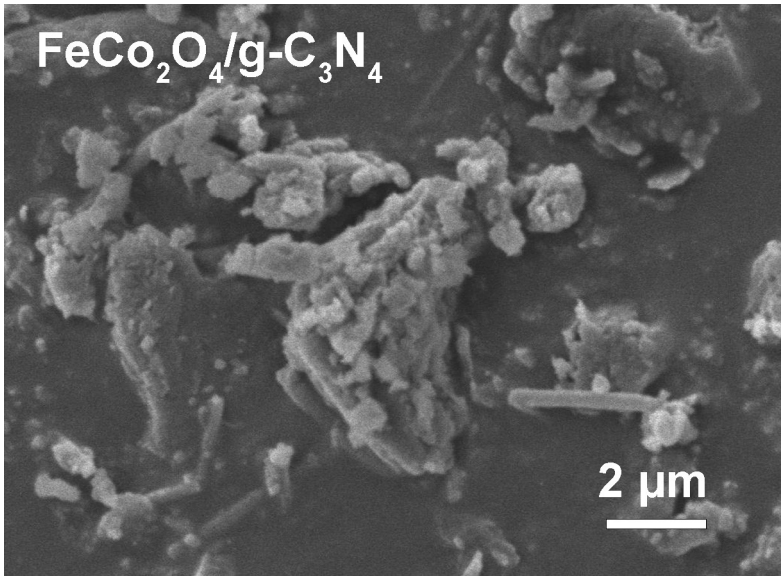

Figure S1. SEM of $FeCo_2O_4$/g-C_3N_4.

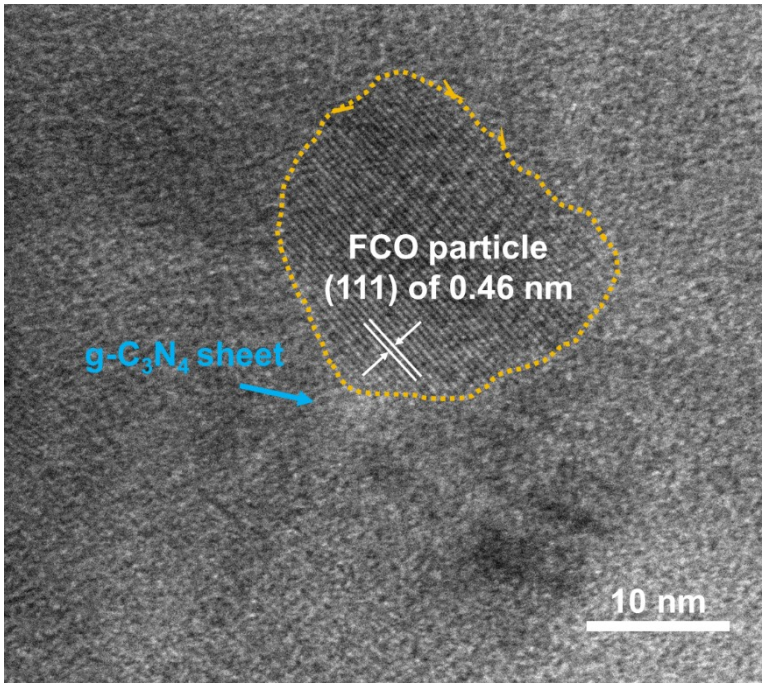

Figure S2. HRTEM image of $FeCo_2O_4$/g-C_3N_4 compositing with $FeCo_2O_4$ nano-particle loaded on g-C_3N_4 nano-sheet.

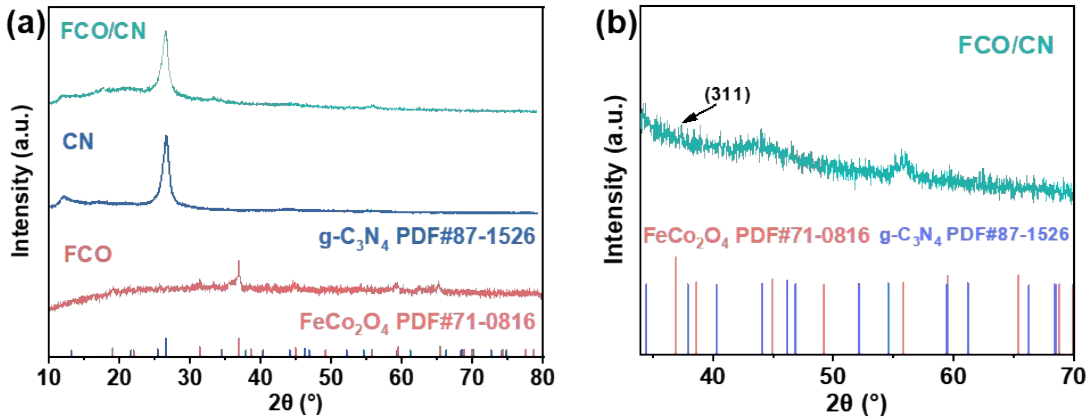

Figure S3. (a) XRD patterns of g-C_3N_4, $FeCo_2O_4$ and $FeCo_2O_4$/g-C_3N_4; (b) Enlarged view of the diffraction peaks for XRD pattern of $FeCo_2O_4$/g-C_3N_4.

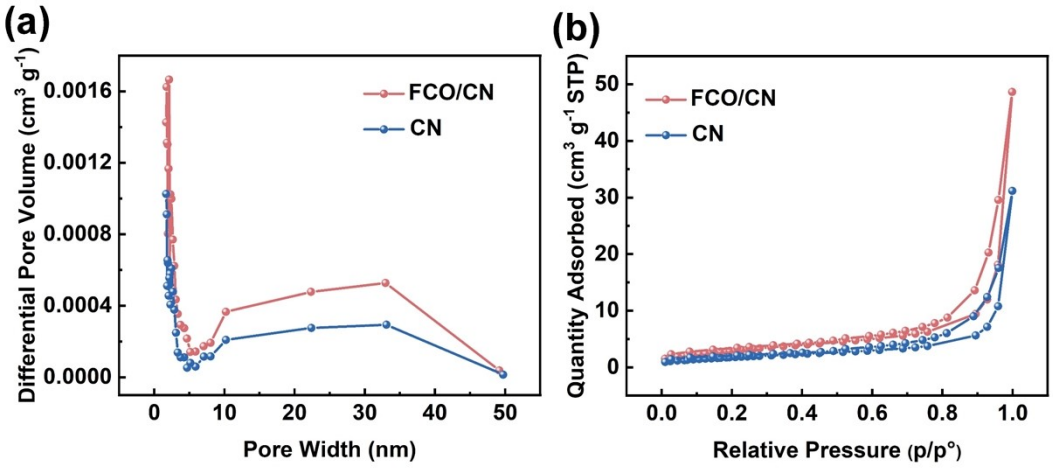

Figure S4. a) N_2 isothermal adsorption and desorption curves and corresponding b) pore-size distribution.

Table S1 Porosity properties from the N_2 adsorption-desorption isotherm of samples.

Samples	V_{total} (cm^3 g^{-1})	S_{BET} (m^2 g^{-1})	$D_{Pore,mean}$ (nm) by BJH
FCO/CN	0.075	11.17	29.14
CN	0.048	6.61	26.95

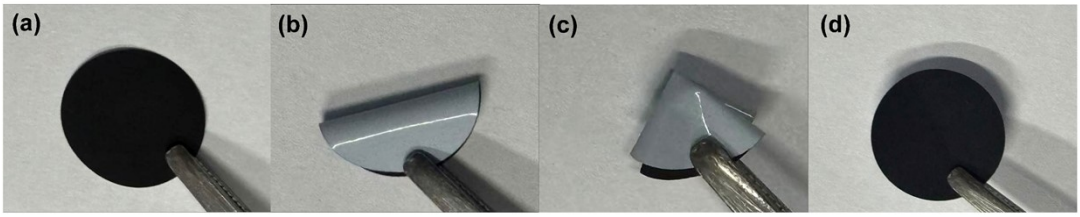

Figure S5. (a-d) Flexibility testing of $FeCo_2O_4$/g-C_3N_4 separator.

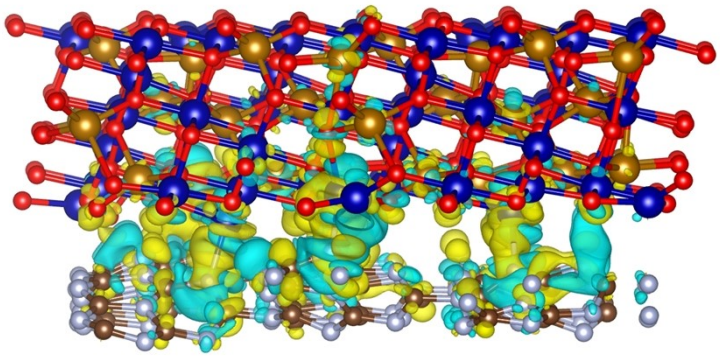

Figure S6. Charge density difference map for the $FeCo_2O_4$/g-C_3N_4 heterojunction.

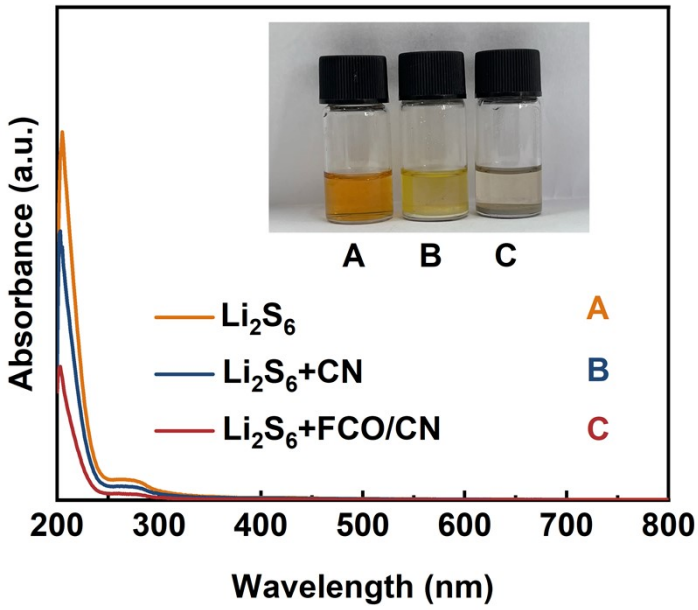

Figure S7. Optical image and UV – vis spectra of Li_2S_6 with adsorption.

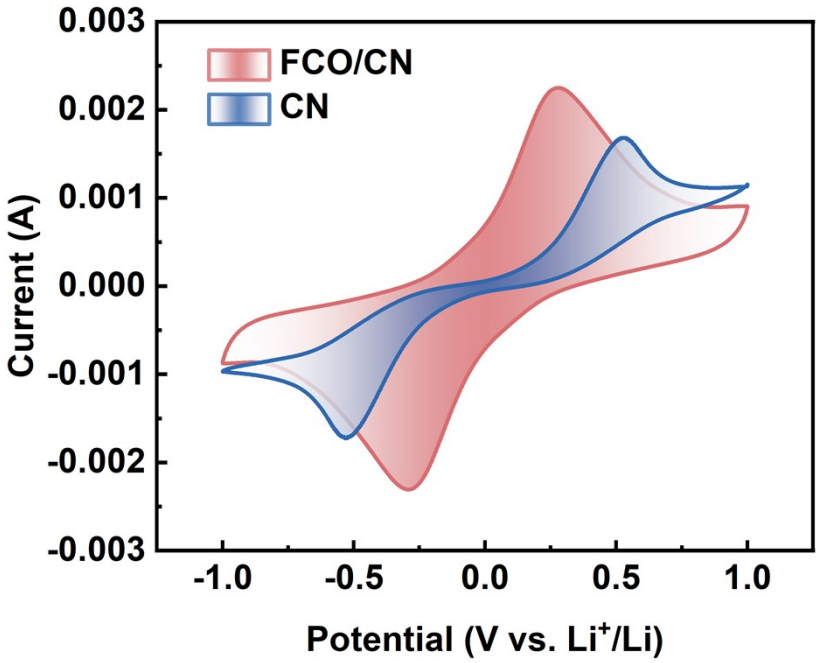

Figure S8. Electrochemical cyclic voltammetry measurements of symmetry cells at scan rate of 0.01 V/s.

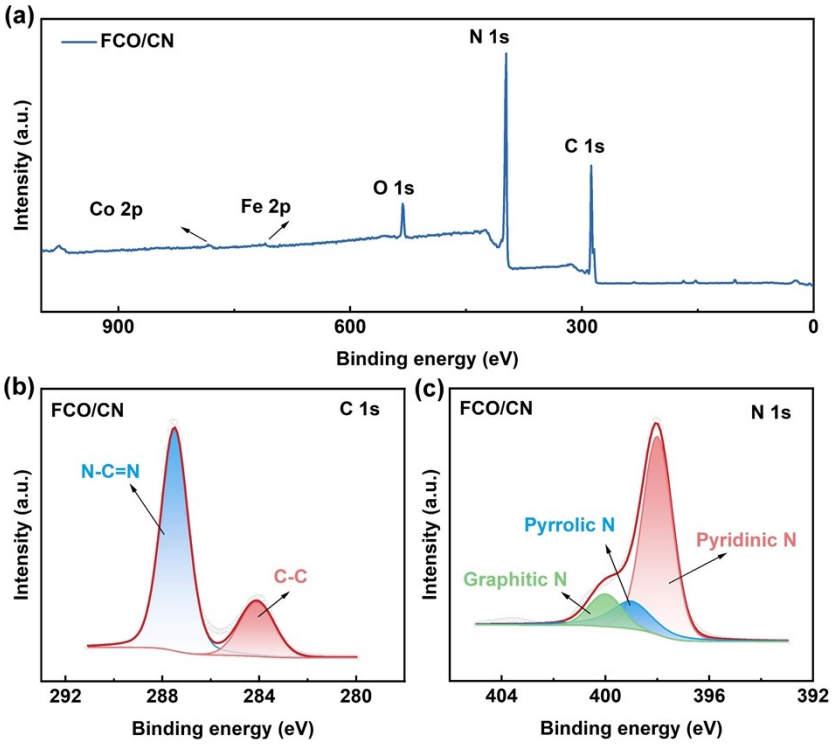

Figure S9. (a) XPS full survey of $FeCo_2O_4$/g-C_3N_4. XPS spectra of (b) C 1s and (c) N 1s in $FeCo_2O_4$/g-C_3N_4.

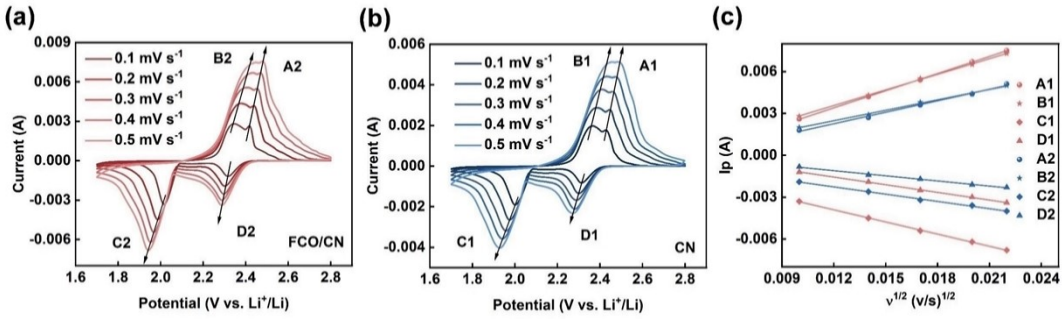

Figure S10. CV curves of the cell with (a) $FeCo_2O_4$/g-C_3N_4 and (b) g-C_3N_4. Linear relationship between Ip and $\nu^{1/2}$ of (c) $FeCo_2O_4$/g-C_3N_4.

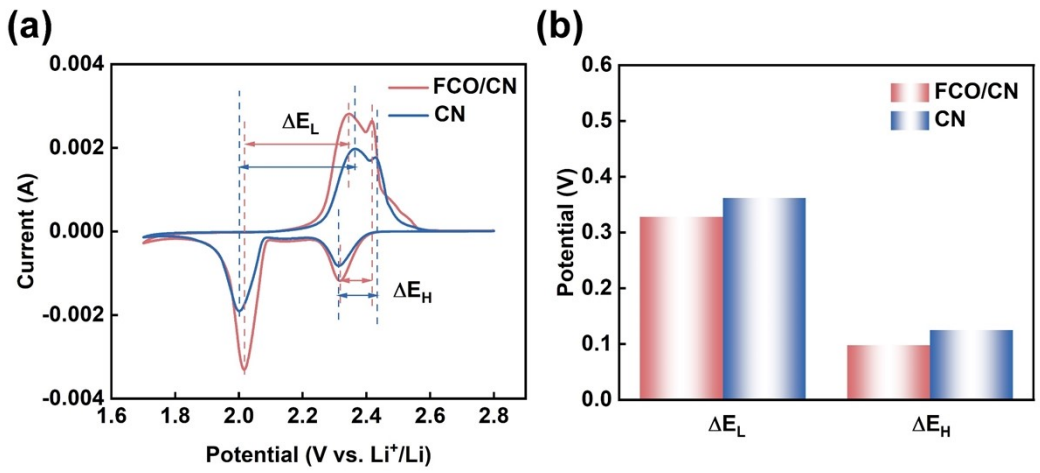

Figure S11. (a) Comparison of CV curves at 0.1 mV s^{-1}. (b) Comparison of ΔE_L and ΔE_H.

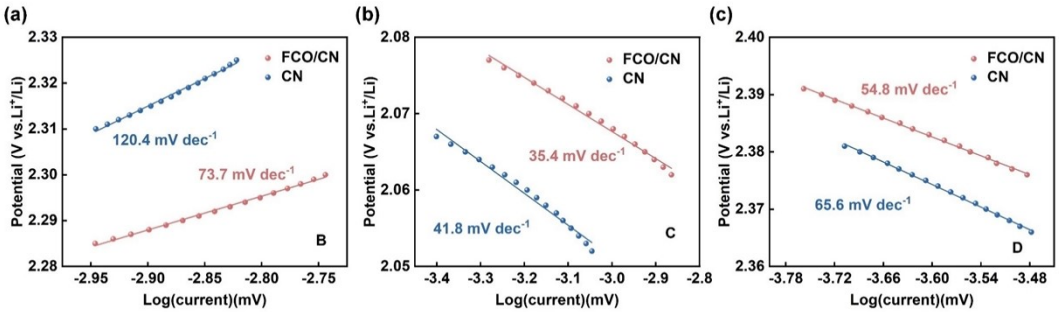

Figure S12. (a-c) Tafel plots derived from redox peaks B, C, and D in the CV profiles measured at a scan rate of 0.1 mv/s.

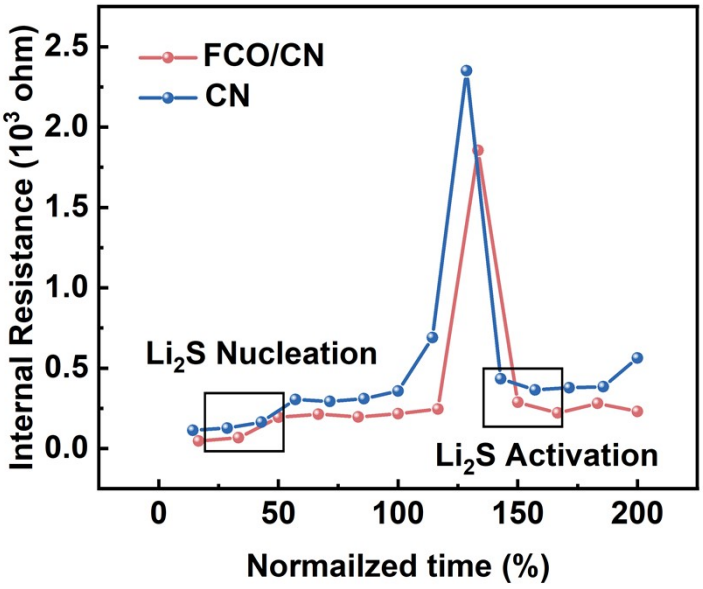

Figure S13. Internal resistance based on GITT.

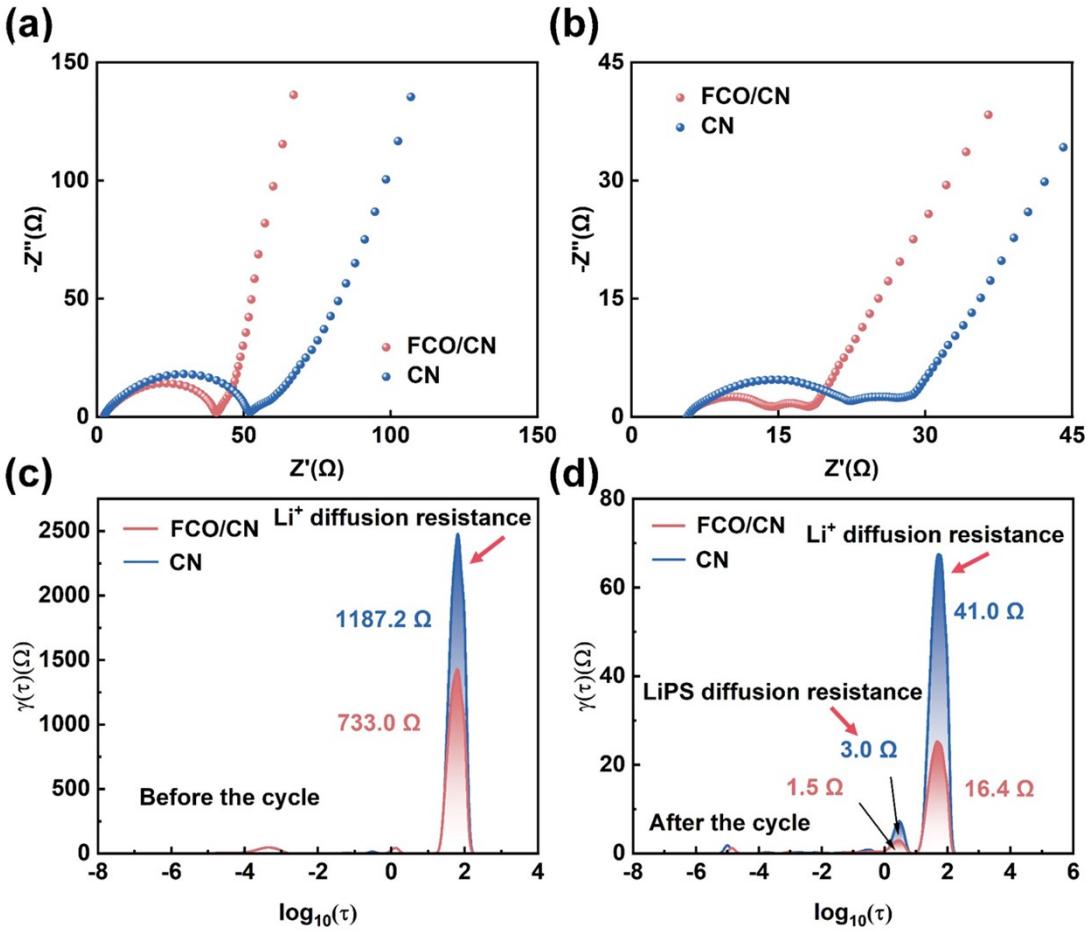

Figure S14. (a) EIS before and (b) after the cycle. (c-d) Discrete impedance spectrum relaxation time plots. The peak at low frequencies ($\tau > 1$ s) is characteristic of Li^+ diffusion processes. The peak in the mid-frequency region ($\tau \approx 10^{-3}$–10^{-1} s) corresponds to the charge transfer resistance associated with the electrocatalytic conversion of lithium polysulfides at the modifier/electrolyte interface. The peak observed in the high-frequency region ($\tau \approx 10^{-5}$–10^{-4} s) is attributed to the ionic transport resistance through the separator coating layer and the contact impedance between the coating and the current collector.

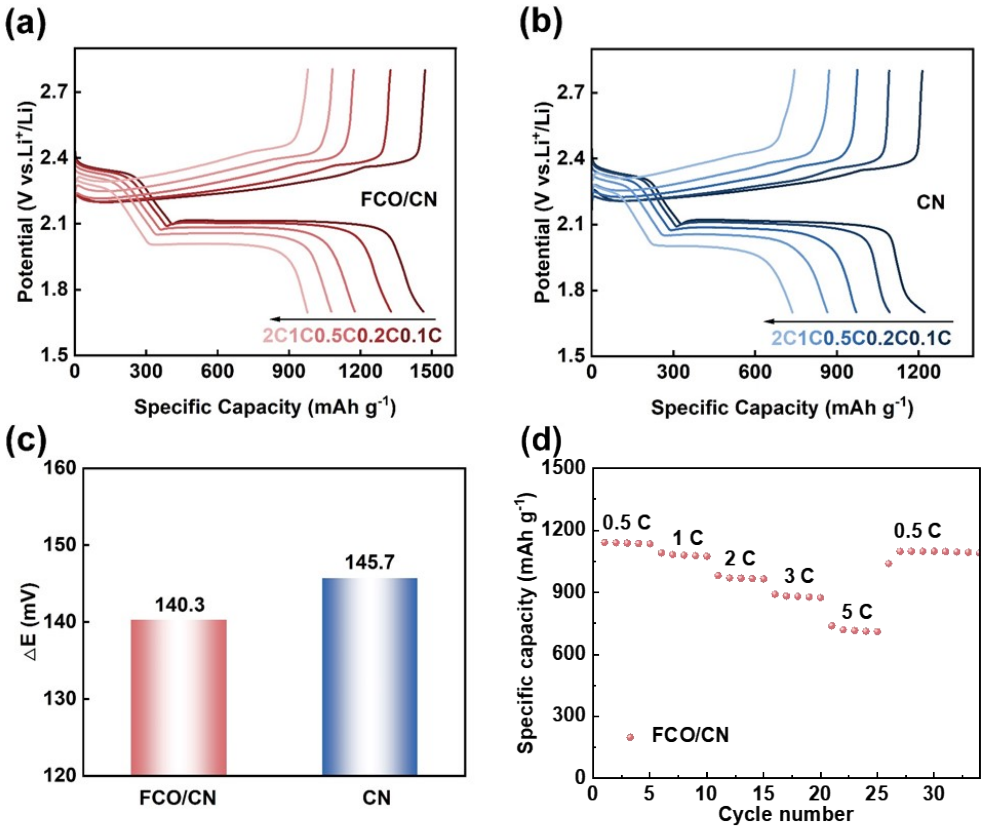

Figure S15. GCD curve of (a) $FeCo_2O_4$/g-C_3N_4 and (b) g-C_3N_4. (c) ΔE from GCD curves of $FeCo_2O_4$/g-C_3N_4 and g-C_3N_4. (d) Rate performance of $FeCo_2O_4$/g-C_3N_4 derived battery regarding higher current densities up-to 5 C.

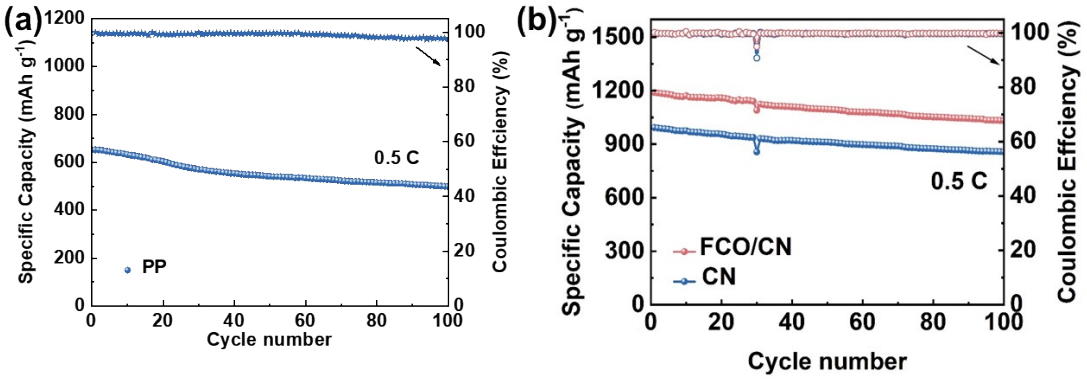

Figure S16. The cyclic performance of an unmodified separator (defied as PP), in comparison with those of FCO/CN and CN.

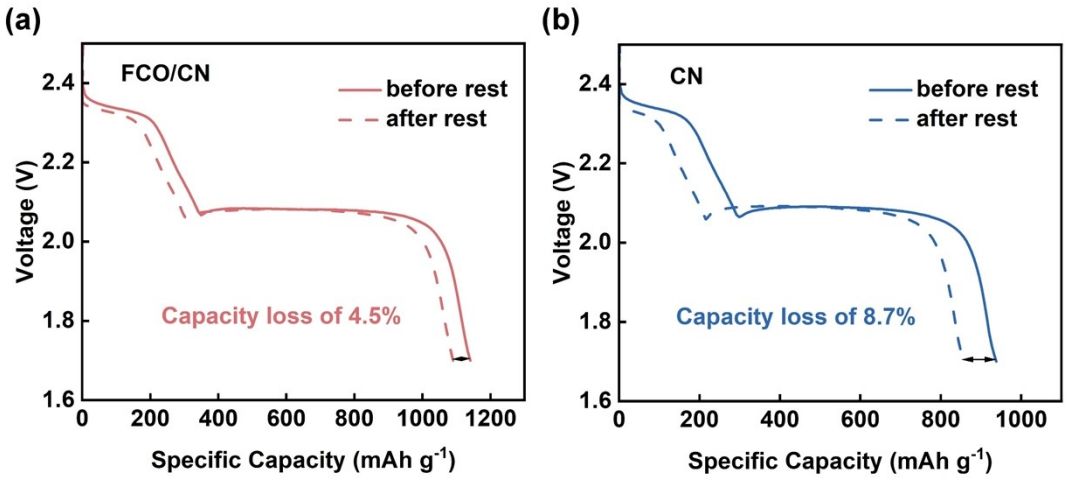

Figure S17. Discharge curves and self-discharge measurement of the cells with (a) $FeCo_2O_4$/g-C_3N_4 and (b) g-C_3N_4.

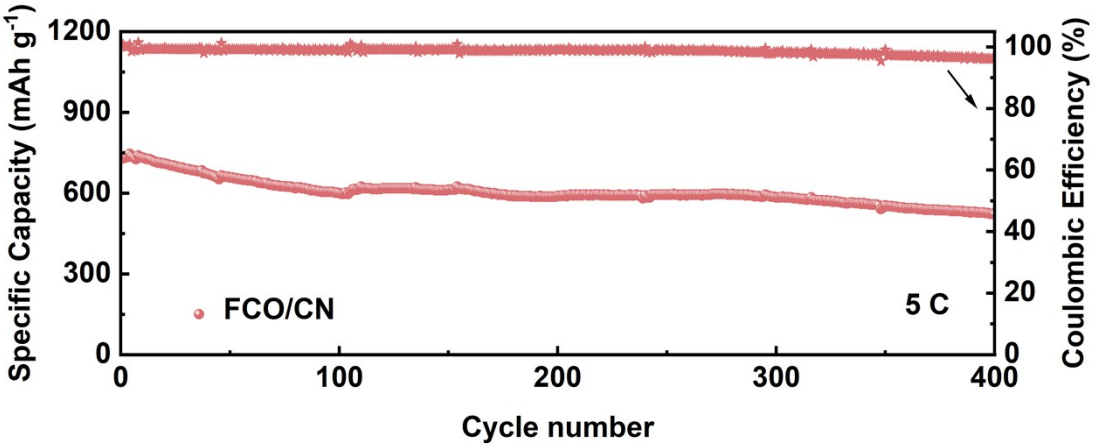

Figure S18. Cycling performance at 5 C.

References

[1] G. Kresse, J. Furthmüller, Efficient iterative schemes for ab initio total-energy calculations using a plane-wave basis set, Physical review B 54 (1996) 11169, https://doi.org/10.1103/PhysRevB.54.11169.

[2] G. Kresse, J. Furthmüller, Efficiency of ab-initio total energy calculations for metals and semiconductors using a plane-wave basis set, Computational materials science 6 (1996) 15-50, https://doi.org/10.1016/0927-0256(96)00008-0.

[3] J. P. Perdew, K. Burke, M. Ernzerhof, Generalized gradient approximation made simple, Physical review letters 77 (1996) 3865, https://doi.org/10.1103/PhysRevLett.77.3865.

[4] P. E. Blöchl, Projector augmented-wave method, Phys. rev. B 50 (1994) 17953-17979, https://doi.org/10.1063/1.5078432.

[5] S. Grimme, J. Antony, S. Ehrlich, H. Krieg, A consistent and accurate ab initio parametrization of density functional dispersion correction (DFT-D) for the 94 elements H-Pu, The Journal of chemical physics 132 (2010), https://doi.org/10.1063/1.3382344.

[6] K. B. Wiberg, C. M. Hadad, T. J. LePage, C. M. Breneman, M. J. Frisch, Analysis of the effect of electron correlation on charge density distributions, The Journal of Physical Chemistry 96 (1992) 671-679, https://doi.org/10.1021/j100181a030.